IEEE Access
Multidisciplinary | Rapid Review | Open Access Journal

Received March 8, 2020, accepted March 18, 2020, date of publication March 24, 2020, date of current version April 8, 2020.

Digital Object Identifier 10.1109/ACCESS.2020.2983076

Loss Estimation of Brushless Doubly-Fed Generator With Hybrid Rotor Considering Multiple Influence Factors

SIYANG YU[1], (Member, IEEE), YUE ZHANG[2], CHANGZHENG CHEN[3], FENGGE ZHANG[1], (Member, IEEE), AND HENG NIAN[4], (Senior Member, IEEE)

[1]School of Electrical Engineering, Shenyang University of Technology, Shenyang 110870, China
[2]School of Electrical Engineering, Shandong University, Jinan 250061, China
[3]School of Mechanical Engineering, Shenyang University of Technology, Shenyang 110870, China
[4]College of Electrical Engineering, Zhejiang University, Hangzhou 310027, China

Corresponding authors : Siyang Yu (yusiyangnuli@163.com) and Yue Zhang (zhangy198810@163.com)

This work was supported in part by the Doctoral Start-up Foundation of Liaoning Province under Project 2019-BS-180, and in part by the National Natural Science Foundation of China under Project 51537007 and Project 51675350.

ABSTRACT The brushless doubly fed generator (BDFG) has been a research focus of wind power generation due to its inherent promising features. Although it is important to consider the effect of losses on the design and analysis of the BDFG, there are a few related comprehensive studies. Moreover, a hybrid rotor is studied to improve the performance of BDFG, which brings greater challenges to the loss calculation. The aim of this paper is to propose the accuracy calculation methods of core loss and copper loss for the studied BDFG with hybrid rotor. The core loss calculation model which taken the influence of harmonics, alternating magnetization, rotating magnetization and two-dimensional magnetic property of material into account is proposed based on the analysis of the magnetic field characteristics. In order to calculate the copper loss considering the skin effect, the inductive current of the assisted cage bars which is difficult to obtain directly is calculated. The accuracy and correctness of the proposed approaches and models are validated by experimental results from a 25kW prototype BDFG with hybrid rotor. In addition, the proposed loss calculation method, especially the core loss calculation model, is also applicable to BDFG with other rotor structure which is operated by the magnetic field modulation mechanism.

INDEX TERMS Brushless doubly fed generator, hybrid rotor, magnetic property, accurate losses model.

I. INTRODUCTION

Recent developments in wind power generation have revitalized research on wind turbine and the problem of how to make wind power system work more efficiently and stably are increasingly prominent [1], [2]. Compared with traditional wind power generators, the brushless doubly fed generator (BDFG) which has the excellent performance of conventional synchronous machine and wound rotor asynchronous machine is more suitable for wind power generation [3], [4]. Moreover, BDFG shows promising features for the field of wind power generation system due to its unique advantages of adjustable power factor, no brush, high reliability, low capacity level of bidirectional inverter, etc., which received much attention of researchers [5], [6].

The associate editor coordinating the review of this manuscript and approving it for publication was Xiaodong Liang.

Unlike conventional AC generators, there are two sets of three-phase symmetrical double-layer windings with different pole numbers and frequencies in the stator slots of BDFG, as shown in Fig. 1. Moreover, one of the stator winding is directly connected to the grid and denoted as the power winding (PW), while the other winding is connected to the grid via a back-to-back converter and denoted as the control winding (CW) [7]. In theory, the direct coupling relationship is non-existent between two sets of stator windings, and the electromechanical energy conversion of BDFG is achieved by the magnetic coupling effect of special rotor [8], [9]. Therefore, the rotor structure has a signification effect on the operating performance of BDFG.

In recent years, as shown in Fig. 2, a cage-assisted magnetic barrier rotor (i.e., hybrid rotor) which has better magnetic field modulation capacity than the commonly used rotors has been proposed [10]–[12]. In [10], the detailed

analytical design approaches based on the magnetic field modulation theory are investigated. The influence of various parameters on the rotor modulating capability was fully considered in the design process. An inductance calculation method based on the modified winding function is proposed for the BDFG with hybrid rotor in [11]. The effects of magnetic layers and cage bars on the air-gap permeance are both considered in the proposed calculation method. In [12], the operating principle and performance of the BDFG with hybrid rotor are illustrated and studied in detail.

In order to accurately evaluate the performance and optimize the design of BDFG, the loss calculation models have been the focus of the BDFG research. In [13], the core and stray load losses of brushless doubly fed induction generators (BDFIG) are calculated and analyzed. In addition, the calculation model is modified according to the magnetic field characteristics of the BDFIG. However, the influence of harmonic losses and rotating magnetization are not considered in the improved core loss calculation model. In [14], an equivalent circuit which considers the stator and rotor core loss of the brushless doubly fed machine (BDFM) is proposed, which improves the estimation of different parameter values, especially the rotor current. In [15], a steady-state equivalent circuit takes core loss into account of BDFM is proposed. In addition, the steady-state torque–speed relations in the presence of core loss are derived by applying energy conservation. A modified equivalent circuit is put forward which incorporates core loss effects for brushless doubly fed reluctance machine (BDFRM) in [16]. In [17], a dynamic model of brushless doubly fed induction machine (BDFIM) in general reference frame in which the core loss is taken into account is proposed. In [18], the analytical expressions for a number of core loss components caused by the complicated operating principle are individually derived. The steady-state electric equivalent circuit model is developed based on the core loss.

According to the above literature, it can be known that the loss calculation is very important for the analysis of motors. However, there are a few related comprehensive studies on loss calculation methods for BDFG. Therefore, it is necessary and important to research the loss calculation for studying the BDFG with hybrid rotor more comprehensively.

In this paper, the core losses calculation model considering the effect of alternating magnetization, rotating magnetization, harmonic magnetic field, and two-dimensional magnetization characteristic is proposed. Meanwhile the calculation method of inductive current in assisted cage bars is derived to calculate the copper losses considering the skin effect. The paper is organized as follows. In Section II, the special structure and detailed prototype parameters of BDFG with hybrid rotor are illustrated. In Section III, the magnetic characteristics of BDFG with hybrid rotor are analyzed in depth. Moreover, the core loss calculation model is presented. In Section IV, the calculation method of cage bar inductive current and copper losses calculation model are proposed and analyzed. Finally, the experimental results of a 25kW prototype BDFG with hybrid rotor are shown in Section V to validate the accuracy and correctness of the proposed models and method.

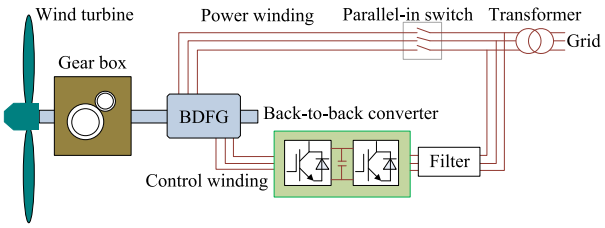

FIGURE 1. Wind turbine system based on the BDFG.

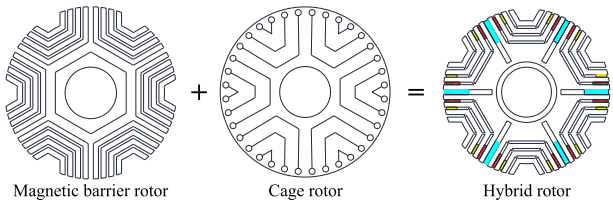

FIGURE 2. Hybrid rotor.

II. STRUCTURE AND OPERATING PRINCIPLE OF BDFG

The BDFG is a new type of speed-adjustable generator composed of two AC feed ports and one common mechanical port, which has two independent three-phase windings with different pole pairs in the same stator, as shown in Fig. 1. The rotor is a special structure couples the stator magnetic fields together [19]. Moreover, the salient poles number of rotor should be equal to the summation of PW and CW pole pair numbers to provide cross-coupling between PW and CW magnetic field [20]. The common rotor structures of BDFG have cage rotor [21], wound rotor [22] and reluctance rotor [23], which all play the role of "poles number converter". Therefore, the rotor structure basically determines the magnetic field modulation capacity which directly affects the performance of BDFG. In order to improve the magnetic field modulation capability, the hybrid rotor is studied in this paper as shown in Fig. 2.

A. STRUCTURE OF BDFG

The two-dimensional model of BDFG with hybrid rotor and the expansion diagram of assisted cage are shown in Fig. 3 and Fig. 4, respectively.

The two sets of windings of BDFG stator adopt strap-wound windings with double-layer short-pitch distribution structure, which can weaken the fifth and seventh harmonic. In addition, the star connection mode is adopted to eliminate third harmonic and its multiple harmonics. Moreover, in order to reduce the core loss of BDFG, the material of stator and rotor all adopt the silicon sheet with low loss coefficient.

B. OPERATING PRINCIPLE

The operating principle of BDFG is also different from the commonly used wind generators. The basic operating

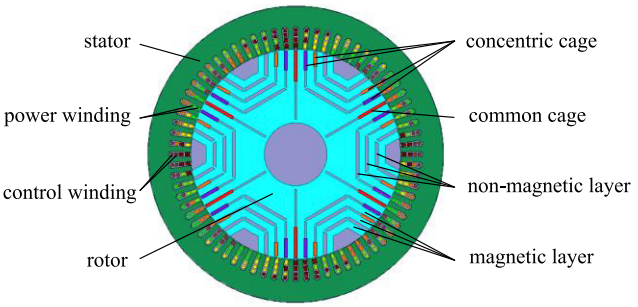

FIGURE 3. The two-dimensional model of BDFG with hybrid rotor.

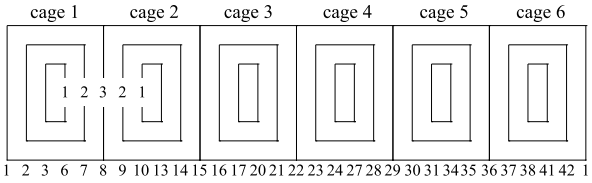

FIGURE 4. Cage bar expansion diagram of novel hybrid rotor.

principle of BDFG is illustrated briefly in this section. As shown in Fig. 1, when the three-phase symmetrical excitation current with the frequency f_c is supplied to the CW, a rotating magnetic field with the number of pole pairs p_c will be generated in the core of BDFG, and the revolution speed n_c can be expressed as:

$$n_c = \frac{60 f_c}{p_c} \tag{1}$$

Thereby, the frequency of rotating magnetic field induced by the CW current in magnetic core of special rotor can be expressed as:

$$f_{cr} = \frac{(n_r \pm n_c)\, p_c}{60} \tag{2}$$

where, n_r denotes the rotor revolution speed. "+" refers to the rotating direction of the n_r is the same with the n_c, while "−" refers to the rotating direction is opposite.

The frequencies of hybrid rotor rotating magnetic field induced by PW and CW are the same due to they share the same rotor, which can be expressed as:

$$f_{cr} = f_{pr} \tag{3}$$

where, f_{pr} denotes the frequency of rotating magnetic field induced by the PW current in magnetic core of special rotor.

The speed of the rotating magnetic field relative to the rotor which is generated by the PW can be written as:

$$n_{pr} = (n_r + n_c)\frac{p_c}{p_p} = n_p - n_r \tag{4}$$

where, p_p and n_p denote the pole pair number of PW and the revolution speed of PW, respectively. Therefore, the frequency of the PW can be deduced through (1) ∼ (4) as:

$$f_p = \frac{n_r\,(p_p + p_c)}{60} \pm f_c \tag{5}$$

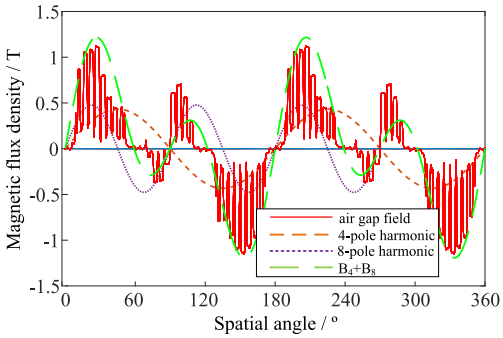

FIGURE 5. The air-gap magnetic density decomposition of BDFG with hybrid rotor ($p_p = 8$, $p_c = 4$).

It can be seen that f_p is only determined by f_c and n_r when the pole pair number of PW and CW are defined. Therefore, the f_p can be kept constant by adjusting f_c under the condition of the unstable wind speed.

III. ANALYSIS AND CALCULATION OF CORE LOSS

The core loss will directly affect the operation efficiency of BDFG. However, the analysis and calculation of core loss is so difficult due to the rich harmonic contents and the irregular distribution of the magnetic field in the core. The specific air-gap magnetic density decomposition of the proposed BDFG (p_p is 8 and p_c is 4) is shown in Fig. 5. It can be seen that although the air-gap magnetic density of the BDFG is mainly composed of 4-pole and 8-pole flux density, there are still many unwanted harmonics. The unwanted harmonics will lead to relatively complex magnetic field characteristics in the core and increase the difficulty of core loss calculation.

A. ANALYSIS OF MAGNETIC FIELD HARMONICS AND MAGNETIZATION CHARACTERISTICS

In order to accurately analyze the magnetic field characteristic of proposed BDFG, some special points are selected in the stator and the rotor as shown in Fig. 6. The magnetic field characteristics are analyzed under different operating conditions (super-synchronous: 1000r/min and sub-synchronous: 400r/min).

The flux density characteristics of the selected positions are shown in Fig. 7 ∼ Fig. 12. In these figures, B1 denotes the stator tooth root, B2 denotes the stator tooth center, B3 denotes the stator tooth head, E1 denotes the position near to stator tooth, E3 and G5 denote the center of their respective magnetic layer.

According to the results, it can be concluded as: 1) There is only radial flux density in stator tooth center, while the stator tooth head and root contain both the radial and tangential flux density. 2) The magnetization mode is approximate to alternating magnetization when the flux density almost just has radial component, while the alternating and rotating magnetization exist simultaneously when the flux density has radial and tangential components. 3) For the flux density of rotor magnetic layer, the radial component accounts for a

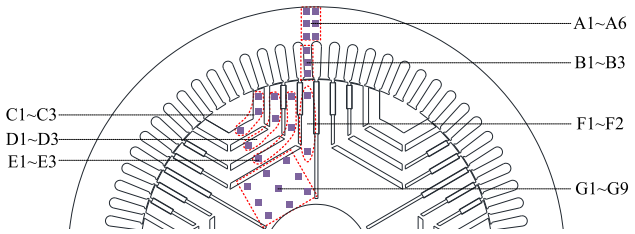

FIGURE 6. The selected special points of BDFG with hybrid rotor.

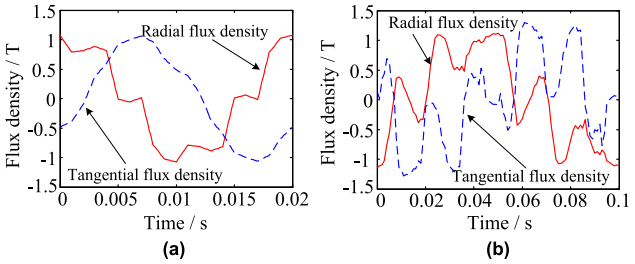

FIGURE 7. Flux density waveform of B1 point. (a) super-synchronous condition (b)sub-synchronous condition.

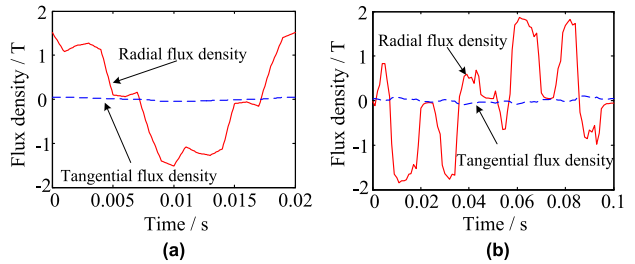

FIGURE 8. Flux density waveform of B2 point. (a) super-synchronous condition (b)sub-synchronous condition.

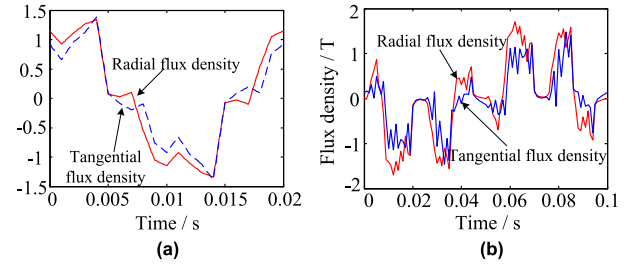

FIGURE 9. Flux density waveform of B3 point. (a) super-synchronous condition (b)sub-synchronous condition.

large proportion, while the tangential component accounts for a small proportion. 4) There are a lot of harmonics in the flux density, especially for the sub-synchronous operating condition. Therefore, in order to accurately calculate the core loss of the BDFG with hybrid rotor, it is necessary to consider the influence of harmonics, alternating magnetization, rotational magnetization and two-dimensional magnetic property of the material together.

B. CORE LOSS CALCULATION MODEL

Among the commonly used mathematical models, the classical core loss separation model only considers alternating

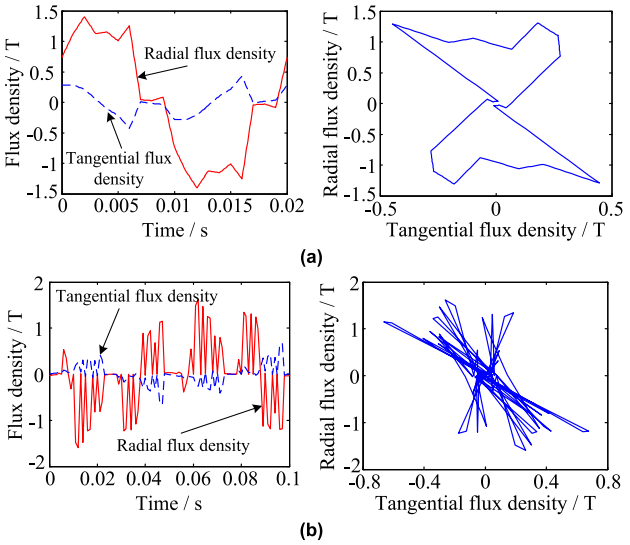

FIGURE 10. Flux density waveform and magnetization locus of E1 point. (a) supper-synchronous condition. (b) sub-synchronous condition.

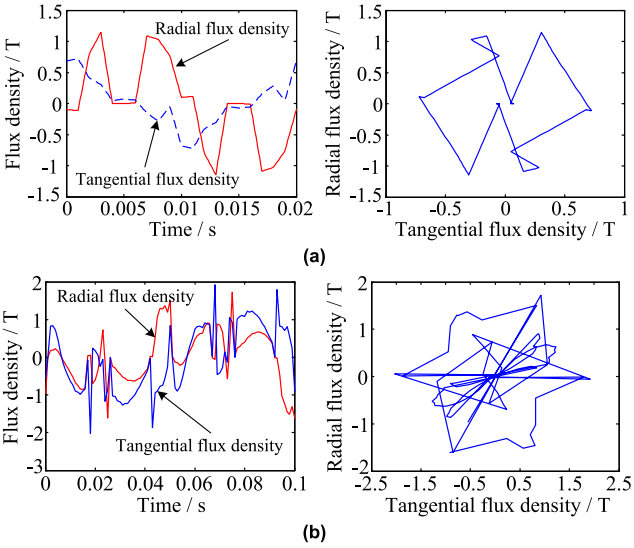

FIGURE 11. Flux density waveform and magnetization locus of E3 point. (a) supper-synchronous condition. (b) sub-synchronous condition.

magnetization, while the elliptic rotation and orthogonal decomposition models can consider alternating and rotating magnetization [24]. However, the magnetic field intensity $\boldsymbol{H}$ is not parallel to the magnetic flux density $\boldsymbol{B}$ in actual core material under the magnetic field of the arbitrary orientation magnetization mode, which is described as the two-dimensional magnetic property. The E&S vector hysteresis model is a mathematical model which can accurately express the relationship between $\boldsymbol{H}$ and $\boldsymbol{B}$ [25]–[27]. However, the traditional E&S vector hysteresis model only can consider the effect of 1st and 3rd harmonics, which does not apply to the condition of BDFG with complex harmonic components. Therefore, in order to further increase the accuracy of core losses calculation, an improved E&S vector hysteresis model which can take more harmonics into account is

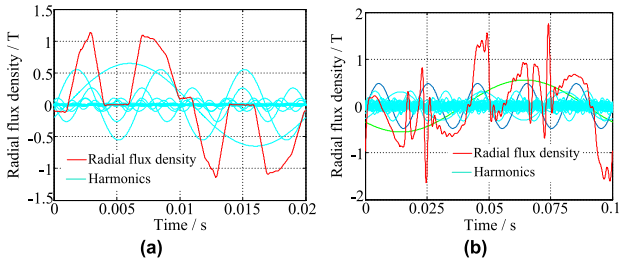

FIGURE 12. Harmonic analysis of radial flux density for G5 point. (a) super-synchronous condition (b) sub-synchronous condition.

proposed. In the proposed improved E&S model, the relationship between $\boldsymbol{B}$ and $\boldsymbol{H}$ can be expressed as:

$$\begin{cases} H_{xh} = \nu_{xrh} B_{xh} + \nu_{xih} \dfrac{\partial B_{xh}}{\partial \tau} \\ H_{yh} = \nu_{yrh} B_{yh} + \nu_{yih} \dfrac{\partial B_{yh}}{\partial \tau} \end{cases} \tag{6}$$

where, the subscript h denotes the order of flux density harmonic. τ denotes the period of one cycle. Subscript x and y denote the coordinate axis direction. In addition, the reluctancy coefficient ν_{krh} and the hysteresis coefficient ν_{kih} can be expressed as:

$$\begin{cases} \nu_{krh} = \dfrac{4}{B_{kh}^2 T} \displaystyle\int_0^T \left[\int_0^{B_{kh}(t)} H_{kh}(t) \cdot \mathrm{d}B_{kh} \right] \mathrm{d}t \\ \nu_{kih} = \dfrac{2}{B_{kh}^2 \omega_h^2 T} \displaystyle\int_0^T H_{kh}(t) \cdot \frac{\mathrm{d}B_{kh}}{\mathrm{d}t} \mathrm{d}t \end{cases} \tag{7}$$

where, the subscript k denotes x and y, T denotes the period of magnetic density waveform, and ω_h denotes the angle velocity of the harmonics.

According to the proposed improved E&S model, the total core loss of BDFG considering alternating magnetization, rotating magnetization, harmonics and two-dimensional magnetic property can be directly calculated by the fundamental terms of obtained B_x, B_y, H_x and H_y without other fitting data, which can increase the correctness in contrast with the commonly used core loss models. The total core loss can be calculated as:

$$p_{\mathrm{Fe}} = \frac{1}{\rho T} \sum_{z=1}^{m} \sum_{h=1}^{n} M_z \int_0^T \left(H_{xzh} \frac{\mathrm{d}B_{xzh}}{\mathrm{d}t} + H_{yzh} \frac{\mathrm{d}B_{yzh}}{\mathrm{d}t} \right) \mathrm{d}t \tag{8}$$

where, m denotes the total number of stator and rotor core elements. n denotes total number of flux density harmonics. ρ denotes the density of silicon steel sheet material. M_z denotes the mass of each element. Subscript z denotes the order of core elements.

IV. ANALYSIS AND CALCULATION OF COPPER LOSS

The copper losses of BDFG with hybrid rotor are mainly concentrated in two sets of windings of stator and the cage bars of hybrid rotor. However, the proposed hybrid rotor cages are non-uniformly distributed and the connection modes are inconsistent, which increases the difficulty of the copper loss calculation. In this section, the copper loss calculation model considering the effect of skin effect is established, the inductive current of the cages which cannot be directly measured are calculated by flux linkage, inductance, current and electromotive force (MMF).

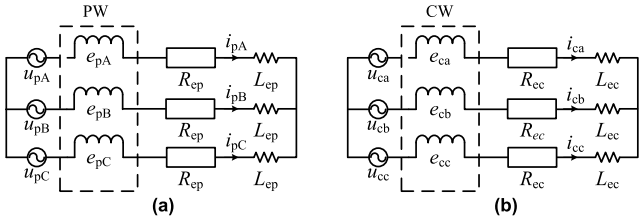

FIGURE 13. The equivalent circuits of stator windings. (a) PW (b) CW.

A. STATOR WINDING

The PW and CW of BDFG with hybrid rotor are made of random coils with a small wire diameter which can neglect skin effect. Moreover, the coupling circuit of the PW and the CW are established as shown in Fig. 13 to further consider the effect of leakage inductance on the stator windings.

In Fig. 13, the subscript A, B, C, a, b, c denote phase winding, u_{p}, R_{ep}, L_{ep} and u_{c}, R_{ec}, L_{ec} denote the voltage, resistance and leakage inductance of the PW and CW overhang, respectively. e_{p}, i_{p} and e_{c}, i_{c} denote the inductive electromotive force (EMF) and phase currents of PW and CW, respectively.

B. ROTOR CAGE BAR

The copper loss of hybrid rotor is mainly produced by the assisted cage bars. The cage bars of rotor adopt single turn pancake copper bar and the frequency of inductive current is high. Therefore, the variation of cage bar resistance and the skin effect cannot be ignored, as shown in Fig. 14. Where, h denotes the height of cage bars.

The skin effect has a significant effect on the AC resistance of rotor cage bars. The increase factor of cage bar resistance caused by skin effect can be expressed as:

$$K_{nk} = \xi_{nk} \frac{\mathrm{sh}2\xi_{nk} + \sin 2\xi_{nk}}{\mathrm{ch}2\xi_{nk} - \cos 2\xi_{nk}} \tag{9}$$

where, the subscript n denotes the order of cage bars. In addition, the cage bar penetration depth can be expressed as:

$$\xi_{nk} = h_n \sqrt{\frac{\pi \mu f_k}{\rho}} \tag{10}$$

where, f_k denotes the k^{th} harmonic frequency of cage bar current. μ and ρ denote the magnetic conductivity and the specific resistance of cage bars, respectively.

The mathematical equivalent for the resistance increase factor of each cage bar considering the influence of various harmonics is treated as:

$$K_{neq} = K_{n0} + a_{n1}^2 K_{n1} + \cdots + a_{nk}^2 K_{nk} \tag{11}$$

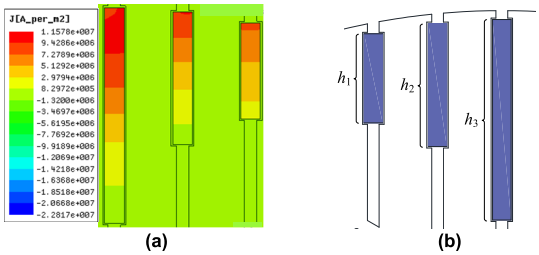

FIGURE 14. Skin effect of rotor cage bars. (a) distribution of cage bar currents density. (b) cage bar penetration depth.

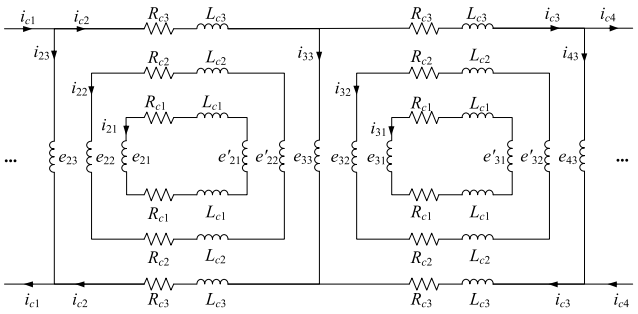

FIGURE 15. Equivalent circuit of hybrid rotor cage bars.

where, K_{n0} and K_{nk} denote AC resistance increase factor under the condition of fundamental current and each harmonic current, respectively. a_{nk} denotes the ratio of each harmonic current to the fundamental current. In addition, subscript k denotes the order of harmonics.

In order to obtain the a_{nk} and K_{req}, the inductive current of cage bars should be calculated and analyzed. The inductive current of cage bar can be calculated by the relationship between the MMF and inductance as:

$$\begin{aligned} e &= -\frac{\mathrm{d}\psi}{\mathrm{d}t} \\ &= -\frac{\mathrm{d}}{\mathrm{d}t}\left(L_{\mathrm{Ar}}i_{\mathrm{A}} + L_{\mathrm{Br}}i_{\mathrm{B}} + L_{\mathrm{Cr}}i_{\mathrm{C}} + L_{\mathrm{ar}}i_{\mathrm{a}} + L_{\mathrm{br}}i_{\mathrm{b}} + L_{\mathrm{cr}}i_{\mathrm{c}}\right) \\ &= -\left(i_{\mathrm{A}}\frac{\mathrm{d}L_{\mathrm{Ar}}}{\mathrm{d}t} + L_{\mathrm{Ar}}\frac{\mathrm{d}i_{\mathrm{A}}}{\mathrm{d}t} + \cdots + i_{\mathrm{c}}\frac{\mathrm{d}L_{\mathrm{cr}}}{\mathrm{d}t} + L_{\mathrm{cr}}\frac{\mathrm{d}i_{\mathrm{c}}}{\mathrm{d}t}\right) \\ &= -\left(i_{\mathrm{A}}\frac{\mathrm{d}L_{\mathrm{Ar}}}{\mathrm{d}\theta_{\mathrm{r}}}\frac{\mathrm{d}\theta_{\mathrm{r}}}{\mathrm{d}t} + L_{\mathrm{Ar}}\frac{\mathrm{d}i_{\mathrm{A}}}{\mathrm{d}t} + \cdots + i_{\mathrm{c}}\frac{\mathrm{d}L_{\mathrm{cr}}}{\mathrm{d}\theta_{\mathrm{r}}}\frac{\mathrm{d}\theta_{\mathrm{r}}}{\mathrm{d}t} + L_{\mathrm{cr}}\frac{\mathrm{d}i_{\mathrm{c}}}{\mathrm{d}t}\right) \\ &= -\left(i_{\mathrm{A}}\omega_{\mathrm{r}}\frac{\mathrm{d}\theta_{\mathrm{r}}}{\mathrm{d}t} + L_{\mathrm{Ar}}\frac{\mathrm{d}i_{\mathrm{A}}}{\mathrm{d}t} + \cdots + i_{\mathrm{c}}\omega_{\mathrm{r}}\frac{\mathrm{d}\theta_{\mathrm{r}}}{\mathrm{d}t} + L_{\mathrm{cr}}\frac{\mathrm{d}i_{\mathrm{c}}}{\mathrm{d}t}\right) \end{aligned} \tag{12}$$

where, L denotes the mutual inductance between the two sets of windings and hybrid rotor cage bars. θ_r denotes mechanical position angle. Subscript r denotes rotor. Furthermore, L can be expressed as [11]:

$$L_{s_i r_j}(\theta_r) = \mu_0 r l \int_{c1}^{c2} g^{-1}(\theta_r, \varphi)\, N_{s_i}(\theta_r, \varphi)\, N_{r_j}(\theta_r, \varphi)\, \mathrm{d}\varphi \tag{13}$$

where, the subscript i and j denote stator windings and rotor cage bar, respectively. r and l denote stator inner diameter and core length, respectively. μ_0 denotes vacuum magnetic conductivity. $g^{-1}(\theta_r, \varphi)$ denotes the calculated air gap function of hybrid rotor. $N_{si}(\theta_r, \varphi)$ and $N_{rj}(\theta_r, \varphi)$ denote winding function of stator windings and rotor cage bars, respectively.

In order to calculate MMF, the equivalent circuit of rotor cage bars is established, as shown in Fig. 15. It should be noted that the produced MMF will also affect the magnetic density characteristics of the air gap.

According to Fig. 15, the circuit equation of two concentric cage of hybrid rotor can be expressed as:

$$\mathrm{e}_{ij} - e'_{ij} = e = 2R_{cj}i_{ij} + 2L_{cj}\frac{\mathrm{d}i_{ij}}{\mathrm{d}t} \tag{14}$$

where, subscript i and j denote rotor slot number and the circuit number in the same concentric cage. e_{ij}, e'_{ij} and i_{ij} denote the voltage drop and current of concentric cage bars on both sides. R_{cj} and L_{cj} denote the end resistance and the end leakage of concentric cage bars.

Similarly, the circuit voltage equation of common cage of hybrid rotor can be expressed as:

$$\begin{cases} e_{i3} - e_{i+1,3} = e = 2R_{\mathrm{c}3}i_{\mathrm{c},i+1} + 2L_{\mathrm{c}3}\dfrac{\mathrm{d}i_{\mathrm{c},i+1}}{\mathrm{d}t} \\ e_{P_r,3} - e_{1,3} = e = 2R_{\mathrm{c}3}i_{\mathrm{c}1} + 2L_{\mathrm{c}3}\dfrac{\mathrm{d}i_{\mathrm{c}1}}{\mathrm{d}t} \end{cases} \quad i = 1, \ldots, p_{\mathrm{r}} - 1 \tag{15}$$

where,

$$i_{\mathrm{c},i+1} = i_{\mathrm{c}i} - i_{i+1,3} \tag{16}$$

In which, e_{i3} and $e_{i+1,3}$ denote the voltage drop of common cage bars on both sides, respectively. $R_{\mathrm{c}3}$ and $L_{\mathrm{c}3}$ denote the end resistance and the end leakage of common cage bars, respectively. $p_{\mathrm{r}} = p_{\mathrm{p}} + p_{\mathrm{c}}$ denotes the pole number of rotor.

C. COPPER LOSS CALCULATION MODEL

Based on the previous description and analysis, the copper loss of BDFG with hybrid rotor can be expressed as:

$$p_{\mathrm{Cu}} = p_{\mathrm{sCu}} + p_{\mathrm{rCu}} \tag{17}$$

where, the stator copper loss p_{sCu} considering the effect of harmonics and rotor cooper loss p_{rCu} considering the effect of skin effect and harmonics, which can be expressed as:

$$p_{\mathrm{sCu}} = 3\sum_{k=1}^{N}\left(I_{\mathrm{pmk}}^2 R_{\mathrm{p}} + I_{\mathrm{cmk}}^2 R_{\mathrm{c}}\right) \tag{18}$$

$$p_{\mathrm{rCu}} = K_{neq}\sum_{k=1}^{N}\sum_{i=1}^{p_{\mathrm{r}}}\left(\sum_{j=1}^{m} I_{ij,k}^2 R_j + I_{i3,k}^2 R_g + 2I_{ci,k}^2 R_{\mathrm{c}3}\right) \tag{19}$$

where, N and k denote the number and order of harmonics, respectively. I_{pm} and I_{cm} denote the root mean square (RMS) current value of PW and CW, respectively. R_{p} and R_{c} denote the resistance of PW and CW, respectively. m denotes the number of concentric cage. $I_{ij,k}$ and $I_{i3,k}$ denote k^{th} current

TABLE 1. Main parameters of prototype BDFG.

Parameter	Value	Parameter	Value
Rated power	25kW	Rated rotating speed	1000
Stator outer diameter	400mm	PW pole pair number	4
Stator inner diameter	285mm	CW pole pair number	2
Rated voltage	380V	Rated frequency of PW	50Hz
Stack length	225mm	Frequency of CW	-20~50Hz
Air gap length	0.5mm	Rotor inner diameter	85mm
Rotor outer diameter	284mm	Magnetic layer number	4

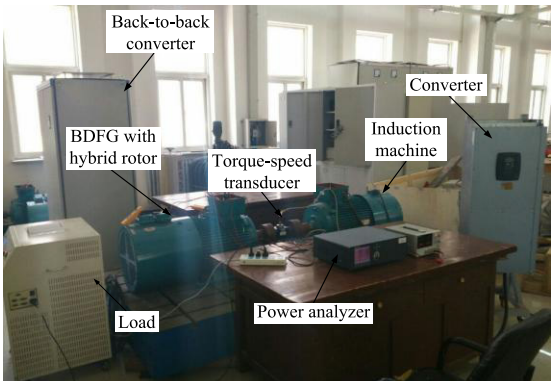

FIGURE 16. Experimental platform of the prototype BDFG.

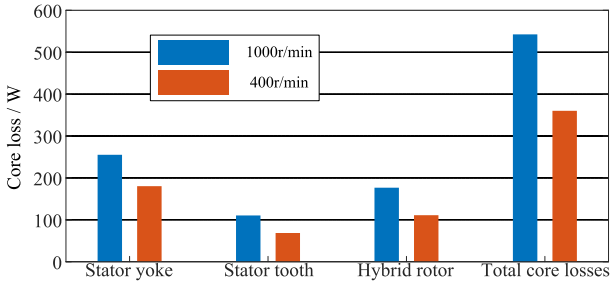

FIGURE 17. Core loss calculation results.

harmonic RMS value of concentric cages and common cage linear parts, respectively. $I_{ci,k}$ denotes k^{th} current harmonic RMS value of common cage end. R_{g} and R_{c3} denote the resistance of common cage linear and end parts.

The resistance of concentric cages R_j can be expressed as:

$$R_j = 2R_{\text{c}j} + 2R_{\text{g}j} \tag{20}$$

where, R_{cj} and R_{gj} denote the resistance of concentric cage end and linear parts, respectively.

V. ANALYSIS OF RESULTS

In order to validate the accuracy of core and copper losses calculation models, a 25kW prototype BDFG is tested. Moreover, the specifications of the prototype are listed in Table 1, and the experimental setup is shown in Fig. 16. In the experimental process, the induction motor is used as prime mover and driven by normal converter.

A. RESULTS ANALYSIS OF LOSSES

Fig. 17 shows the core loss results of stator yoke, stator tooth and hybrid rotor calculated by the proposed improved

TABLE 2. Units for magnetic properties.

	Rotating speed	Load power (6kW)	Load power (10kW)
Calculated value	400r/min	252.09W	458.03W
	1000r/min	216.49W	345.30W
Simulated value	400r/min	228.96W	415.26W
	1000r/min	196.99W	314.49W

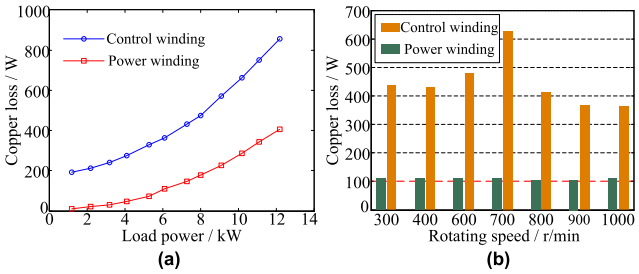

FIGURE 18. Copper losses. (a) different load power at constant speed of 1000r/min. (b) different rotating speed at constant load power of 6kW.

E&S model. Moreover, it can be seen that the core loss of stator yoke, stator tooth and hybrid rotor under the supper-synchronous condition (1000r/min) are always higher than that under the sub-synchronous condition (400r/min). This is because the frequency of excitation current which is one of the main frequencies is smaller under the sub-synchronous condition. For the total core loss, the stator core loss accounts for the majority which is about twice as much as that of the rotor core loss. In addition, the core loss of stator tooth is smaller than that of stator yoke.

Based on the proposed copper loss calculation model, Fig. 18 shows the variation condition of stator windings under different load and different operating speed, and Table 2 gives the copper loss values of hybrid rotor cage bars under two operating modes.

According to the results, it can be obtained the following conclusions as:

(1) The copper loss of PW and CW increase significantly with the increasing of load power under the same speed.

(2) In any case, the copper loss of CW is much larger than that of PW.

(3) Under different speed, the copper loss of PW basically remains unchanged due to the constant frequency, while the copper loss of CW increases first and then decreases with the increasing of speed.

(4) The skin effect of the current has a signification effect on the copper loss of the cage bar.

(5) The calculated value of cage bar copper loss is about 10% higher than the simulated value, which mainly also because the influence of skin effect is not considered in the simulation.

B. EXPERIMENTAL VERIFICATION

Due to the limited conditions, the induced current value of the assisted cage bars in the hybrid rotor cannot be directly measured through experiments. In addition, the magnetic

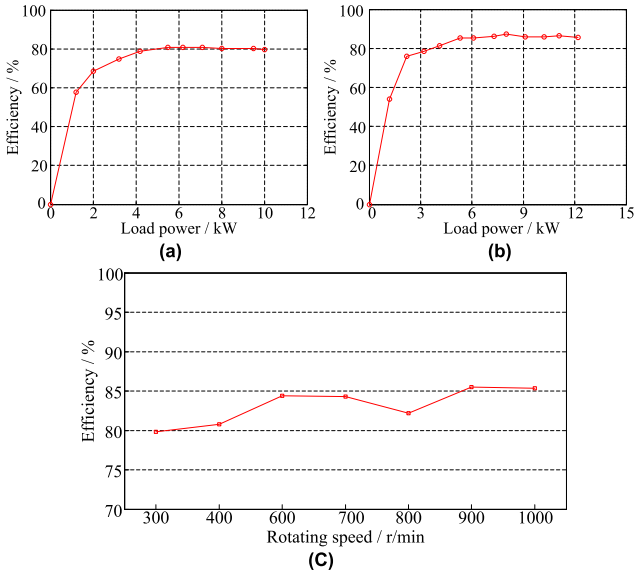

FIGURE 19. Experimental efficiency. (a) sub-synchronous operating (400r/min). (b) supper-synchronous operating (1000r/min). (c) different rotating speeds with the same load power of 10kW.

TABLE 3. Comparison of experimental and calculation efficiencies.

	Model calculation		Experiment	
	1000r/min	400r/min	1000r/min	400r/min
Efficiency	88.148%	82.951%	85.798%	79.577%
Error	2.350%	3.374%	0	0

field of BDFG is very complicated and includes many harmonics, so it is difficult to directly separate core loss through experiment. Therefore, the efficiency is used to indirectly verify the correctness of the proposed core and copper loss calculation models. Furthermore, the different operating modes have different efficiency calculation methods [14]. In sub-synchronous condition, the power of CW is regarded as input power. While in super-synchronous condition, the power of CW is regarded as output power.

Fig. 19 shows the experimental efficiencies under the different operating modes. It can be seen that the efficiency of supper-synchronous operating condition is higher than that of sub-synchronous operating condition. Therefore, in order to improve the efficiency of wind power generation system with BDFG, it is better to make the BDFG operate in super-synchronous condition.

The comparison results of the measured efficiency by experiment and the calculated efficiency by the proposed loss calculation models are shown in Table 3. For the comparison, the output power of PW both are 10kW. In addition, for the calculated efficiency values, the mechanical loss and stray loss are considered and calculated by the commonly used approximate formulas.

According to the results of Table 3, it can be known that the error between the experimental values and the calculated values is small, which fully demonstrates the correctness and feasibility of the calculation methods of core loss and copper loss proposed in this paper.

VI. CONCLUSION

In this paper, the core loss and copper loss of the hybrid rotor BDFG with superior performance are analyzed in detail. The magnetic field characteristics of stator yoke, stator tooth and hybrid rotor are investigated deeply. An improved E&S core loss calculation model which can take the effect of harmonics, alternating magnetization, rotating magnetization and two-dimensional magnetic property into account is proposed. The inductive current of assisted cage bars is calculated based on the law of electromagnetic induction. The copper loss calculation model considering the influence of skin effect is presented. In order to verify the effectiveness and correctness of the proposed losses calculation models, the calculated efficiency based on the losses calculation models has been compared with experimental results of a prototype BDFG with hybrid rotor. The results indicate that the proposed models can accurately estimate the core and copper losses of BDFG with hybrid rotor. Furthermore, the characteristics core losses and copper losses are summarized by the simulation and experimental results.

REFERENCES

[1] M. Liserre, R. Cardenas, M. Molinas, and J. Rodriguez, "Overview of multi-MW wind turbines and wind parks," *IEEE Trans. Ind. Electron.*, vol. 58, no. 4, pp. 1081–1095, Apr. 2011.
[2] H. Li and Z. Chen, "Overview of different wind generator systems and their comparisons," *IET Renew. Power Gener.*, vol. 2, no. 2, pp. 123–138, Jun. 2008.
[3] Y. Jiang, J. Zhang, and T. Li, "A permanent magnet brushless doubly fed generator with segmented structure," *IEEE Trans. Magn.*, vol. 54, no. 3, Mar. 2018, Art. no. 8700204.
[4] L. Zhu, F. Zhang, S. Jin, S. Ademi, X. Su, and W. Cao, "Optimized power error comparison strategy for direct power control of the open-winding brushless doubly fed wind power generator," *IEEE Trans. Sustain. Energy*, vol. 10, no. 4, pp. 2005–2014, Oct. 2019.
[5] P. Han, M. Cheng, Y. Jiang, and Z. Chen, "Torque/Power density optimization of a dual-stator brushless doubly-fed induction generator for wind power application," *IEEE Trans. Ind. Electron.*, vol. 64, no. 12, pp. 9864–9875, Dec. 2017.
[6] J. Zhang, Y. Jiang, X. Hu, and S. Xu, "A brushless doubly fed generator based on permanent magnet field modulation," *IEEE Trans. Ind. Electron.*, vol. 67, no. 5, pp. 3505–3516, May 2020.
[7] A. M. Knight, R. E. Betz, and D. G. Dorrell, "Design and analysis of brushless doubly fed reluctance machines," *IEEE Trans. Ind. Appl.*, vol. 49, no. 1, pp. 50–58, Jan. 2013.
[8] H. Gorginpour, H. Oraee, and R. A. McMahon, "Electromagnetic-thermal design optimization of the brushless doubly fed induction generator," *IEEE Trans. Ind. Electron.*, vol. 61, no. 4, pp. 1710–1721, Apr. 2014.
[9] D. G. Dorrell, A. M. Knight, W. K. Song, and R. E. Betz, "Saturation and ducting effects in a brushless doubly-fed reluctance machine," *IEEE Trans. Magn.*, vol. 49, no. 7, pp. 3933–3936, Jul. 2013.
[10] F. Zhang, S. Yu, Y. Wang, S. Jin, and M. G. Jovanovic, "Design and performance comparisons of brushless doubly fed generators with different rotor structures," *IEEE Trans. Ind. Electron.*, vol. 66, no. 1, pp. 631–640, Jan. 2019.
[11] S. Yu, F. Zhang, and H. Wang, "Parameter calculation and analysis of a novel wind power generator," *IEEE Trans. Magn.*, vol. 53, no. 11, Nov. 2017, Art. no. 8205607.
[12] F. Zhang, S. Yu, X. Wang, H. Wang, and S. Jin, "Research of a novel brushless doubly-fed generator with hybrid rotor," *IEEE Trans. Appl. Supercond.*, vol. 26, no. 7, Oct. 2016, Art. no. 0608205.
[13] H. Gorginpour, H. Oraee, and E. Abdi, "Calculation of core and stray load losses in brushless doubly fed induction generators," *IEEE Trans. Ind. Electron.*, vol. 61, no. 7, pp. 3167–3177, Jul. 2014.

[14] M. N. Hashemnia, F. Tahami, and E. Oyarbide, "Investigation of core loss effect on steady-state characteristics of inverter fed brushless doubly fed machines," *IEEE Trans. Energy Convers.*, vol. 29, no. 1, pp. 57–64, Mar. 2014.
[15] M. N. Hashemnia, F. Tahami, P. Tavner, and S. Tohidi, "Steady-state analysis and performance of a brushless doubly fed machine accounting for core loss," *IET Electr. Power Appl.*, vol. 7, no. 3, pp. 170–178, Mar. 2013.
[16] I. Scian, D. G. Dorrell, and P. J. Holik, "Assessment of losses in a brushless doubly-fed reluctance machine," *IEEE Trans. Magn.*, vol. 42, no. 10, pp. 3425–3427, Oct. 2006.
[17] H. Mosaddegh Hesar, H. A. Zarchi, and G. A. Markadeh, "Modeling and dynamic performance analysis of brushless doubly fed induction machine considering iron loss," *IEEE Trans. Energy Convers.*, vol. 35, no. 1, pp. 193–202, Mar. 2020.
[18] M. Yousefian, H. A. Zarchi, and H. Gorginpour, "Modified steady-state modelling of brushless doubly-fed induction generator taking core loss components into account," *IET Electr. Power Appl.*, vol. 13, no. 9, pp. 1402–1412, Sep. 2019.
[19] F. Barati, S. Shao, E. Abdi, H. Oraee, and R. Mcmahon, "Generalized vector model for the brushless doubly-fed machine with a nested-loop rotor," *IEEE Trans. Ind. Electron.*, vol. 58, no. 6, pp. 2313–2321, Jun. 2011.
[20] S. Khaliq, S. Atiq, T. A. Lipo, and B.-I. Kwon, "Rotor pole optimization of novel axial-flux brushless doubly fed reluctance machine for torque enhancement," *IEEE Trans. Magn.*, vol. 52, no. 7, Jul. 2016, Art. no. 8106204.
[21] H. Gorginpour, H. Oraee, and B. Jandaghi, "A novel rotor configuration for brushless doubly-fed induction generators," *IET Electr. Power Appl.*, vol. 7, no. 2, pp. 106–115, Feb. 2013.
[22] C. Kan, T. Ren, and Y. Hu, "Design and experimental analysis of a wound brushless doubly fed machine based on a rotor with the reluctance effect," *IET Electr. Power Appl.*, vol. 13, no. 4, pp. 551–558, Apr. 2019.
[23] M.-F. Hsieh, Y.-H. Chang, and D. G. Dorrell, "Design and analysis of brushless doubly fed reluctance machine for renewable energy applications," *IEEE Trans. Magn.*, vol. 52, no. 7, Jul. 2016, Art. no. 8204705.
[24] S. Zhu, M. Cheng, J. Dong, and J. Du, "Core loss analysis and calculation of stator permanent-magnet machine considering DC-biased magnetic induction," *IEEE Trans. Ind. Electron.*, vol. 61, no. 10, pp. 5203–5212, Oct. 2014.
[25] Y. Zhang, Y. Liu, Y. Li, D. Xie, and B. Bai, "A complex-valued rotating magnetic property model and its application to iron core loss calculation," *IEEE Trans. Magn.*, vol. 50, no. 2, pp. 397–400, Feb. 2014.
[26] M. Enokizono, H. Shimoji, and T. Horibe, "Loss evaluation of induction motor by using magnetic hysteresis E&S^2 model," *IEEE Trans. Magn.*, vol. 38, no. 5, pp. 2379–2381, Sep. 2002.
[27] N. Soda and M. Enokizono, "Improvement of T-joint part constructions in three-phase transformer cores by using direct loss analysis with E&S model," *IEEE Trans. Magn.*, vol. 36, no. 4, pp. 1285–1288, Jul. 2000.

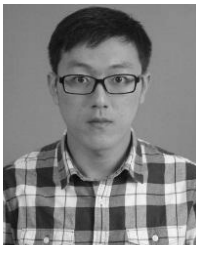

SIYANG YU (Member, IEEE) received the B.Eng., M.Sc., and Ph.D., degrees from the Shenyang University of Technology, Shenyang, China, in 2011, 2014, and 2018, respectively, all in electrical engineering, and the M.Sc. degree in mechatronics from Kyungsung University, Busan, South Korea, in 2014. He is currently a Postdoctoral Researcher with the School of Electrical Engineering, Shenyang University of Technology. He has authored or coauthored more than 30 journal and conference papers. His research interests include design, analysis, and control of electrical machines for industrial applications.

YUE ZHANG was born in Shenyang, China. He received the B.Eng. degree from the Shenyang University of Technology, Shenyang, in 2011, the M.Eng. degree from Zhejiang University, Hangzhou, China, in 2014, and the Ph.D. degree from Queen's University Belfast, Belfast, U.K., in 2018.

Since 2019, he has been with Shandong University, where he is currently a Professor. His research interest includes the design and analysis of electrical machines for industrial applications and electrical vehicles.

CHANGZHENG CHEN received the B.Eng. degree from Jilin University, Changchun, China, in 1986, the M.Eng. degree from Northeastern University, Shenyang, China, in 1991, and the Ph.D. degree from the China University of Mining and Technology, Xuzhou, China, in 1998. Since 1998, he has been with the Shenyang University of Technology. In 1998, he was promoted to an Associate Professor. Since 2001, he has been a Full Professor. He has authored or coauthored more than 150 articles and holds numerous issued/pending patents. He has chaired and participated in the National and Provincial Natural Science Foundation. His research interests include fault information processing, mechanical fault diagnosis, vibration, and noise control.

FENGGE ZHANG (Member, IEEE) received the B.E.E., M.S., and Ph.D. degrees from the Shenyang University of Technology, Shenyang, China, in 1984, 1990, and 2000, respectively, all in electrical engineering. Since 1984, he has been with the School of Electrical Engineering, Shenyang University of Technology, where he is currently a Professor. From October 2001 to July 2002, he was a Visiting Scholar with the Esslingen University of Applied Sciences, Esslingen, Germany. He has published numerous journal and conference papers on electrical machines and control systems. His research and teaching interests include electro-magnetic theory, dynamic simulation, magnetic field analysis, optimized design, computer control technology of electrical machines, and wind power generating systems.

HENG NIAN (Senior Member, IEEE) received the B.Eng. and M.Eng. degrees from the Hefei University of Technology, China, and the Ph.D. degree from Zhejiang University, China, in 1999, 2002, and 2005 respectively, all in electrical engineering.

From 2005 to 2007, he was a Postdoctoral Researcher with the College of Electrical Engineering, Zhejiang University, China. In 2007, he was promoted as an Associate Professor. Since 2016, he has been a Full Professor with the College of Electrical Engineering, Zhejiang University, China. From 2013 to 2014, he was a Visiting Scholar with the Department of Electrical, Computer, and System Engineering, Rensselaer Polytechnic Institute, Troy, NY. He has published more than 40 IEEE/IET Transaction papers and holds more than 20 issued/pending patents. His current research interests include the optimal design and operation control for wind power generation systems.